imaging, because of its advantages of high sensitivity, good spatial resolution, quantitative results, and ease of probe development.

DEVELOPMENT OF AMYLOID-IMAGING AGENTS

Recent advances in molecular imaging have enabled the noninvasive detection of amyloid deposits by PET or SPECT. For the high-contrast detection of amyloid deposits, imaging agents should have high binding affinity for Aβ fibrils and substantial permeability through the blood–brain barrier (BBB). Several amyloid-binding agents have been developed for the *in vivo* detection of amyloid deposits (Fig. (2)). The development of these agents started with the use of Congo red, which is commonly used for the histochemical staining of amyloid [4]. However, the BBB permeability of Congo red is limited because of its molecular size and electrostatic charge. Therefore, several Congo red derivatives have been developed with improved BBB permeability without reduced binding to amyloid [5-8]. Chrysamine-G is the first Congo red derivative that has been examined as an *in vivo* amyloid-imaging probe. However, entry of this compound into the brain is limited. Other derivatives, including BSB, ISB, and methoxy-X04, have also been developed to improve the BBB permeability. BSB successfully visualizes brain amyloid deposits in APP-transgenic mice after intravenous administration of the

compound. However, this compound has insufficient BBB permeability for it to be useful as a clinical PET tracer. The first successful amyloid imaging agent to have been administered to humans is 2-(1-{6-[(2-[18F]fluoroethyl)(methyl)amino]-2-naphthyl}ethylidene)malononitrile ([18F]FDDNP) [9]. One of the characteristics of this agent is its ability to bind both SPs and NFTs in the AD brain. In addition, this compound is extremely lipophilic; therefore, it can penetrate the BBB more easily than previously reported compounds [10]. Interestingly, this compound binds to the same site in Aβ fibrils as non-steroidal anti-inflammatory drugs (NSAIDs) do. Therefore, this agent enables us to determine the occupancy rate of NSAIDs and experimental drugs in SPs [11]. Other candidate amyloid-imaging agents include thioflavin-T derivatives [12, 13]. N-methyl-[11C]2-(4'-methylaminophenyl)-6-hydroxybenzothiazole ([11C]PIB) is one such derivative and is currently the most successful amyloid-imaging agent. This compound shows high binding affinity for Aβ fibrils and SPs in AD brain homogenates, in contrast to low binding affinity for NFTs [14]. After intravenous administration, this agent shows high BBB permeability and rapid washout from normal brain tissue. Other amyloid-imaging agents, such as IMPY, stilbene, benzofuran, and acridine orange derivatives, have also been explored for use as PET and SPECT imaging probes [15-19]. The iodinated agent IMPY has been explored as a SPECT
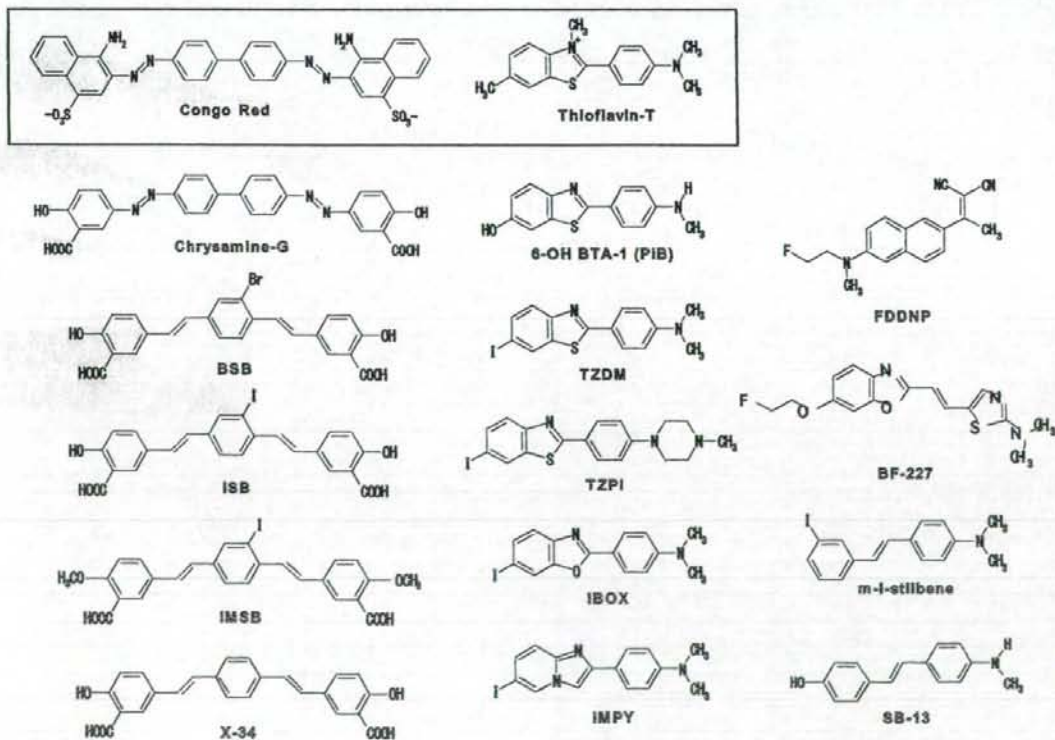

Fig. (2). Chemical structures of common imaging probes for amyloid plaques.

imaging agent and has been used in humans. Other iodinated agents are also under evaluation.

Benzoxazole derivatives are other possible amyloid-imaging agents [20-23]. Their chemical structures, binding affinities for Aβ fibrils, and pharmacokinetic data are summarized in Table 1. Most of these compounds show high binding affinity for both Aβ1-40 and Aβ1-42 fibrils. BF-191 and BF-208, which have halogens as substituents for amino groups, show low affinity for both Aβ1-40 and Aβ1-42 fibrils, suggesting that amino groups have a crucial role in binding to Aβ fibrils. All compounds have good BBB permeability. BF-227 shows faster washout from normal brain tissue than the other compounds [23, 24]. BF-227 distinctly stained SPs during the neuropathological staining of AD brain sections, and this staining pattern correlated well with Aβ immunostaining (Fig. (3)). Fluorescence microscopy revealed that this agent binds preferentially to SPs rather than NFTs. An acute and subacute toxicity study of BF-227 indicated sufficient safety for clinical use as a PET probe.

HUMAN PET STUDY

Human amyloid imaging was first studied using [18F]FDDNP [9]. A [18F]FDDNP PET study revealed regional accumulation of [18F]FDDNP in the SP- and NFT-rich areas of the brain [25]. Global FDDNP-PET binding distinctly differentiated AD patients from normal subjects. FDDNP retention in the medial temporal lobes of subjects with mild cognitive impairment (MCI) was intermediate between levels in AD patients and normal control subjects. This finding is consistent with the observation in an autopsy study that the concentration of NFTs in the medial temporal lobes was intermediate between that in normally aging subjects and AD patients [26]. These binding characteristics indicate that this imaging agent is useful in tracing the progression of AD from the MCI stage. In addition, this agent has the potential to differentiate atypical prion disease from AD [27]. The weakness of this agent is the low signal-to-background ratio of the images, which is due to the considerable amount of nonspecific accumulation in normal brain tissue [28].

In comparison with [18F]FDDNP, [11C]PIB PET images differentiated AD patients from normal individuals more distinctly [29]. PIB retention was observed in the SP-rich neocortex of the brain but not in the NFT-rich medial temporal cortex, indicating that this agent binds selectively to SPs. A quantitative imaging method using PIB has already been validated [30, 31]. Over half the subjects with MCI also showed neocortical PIB accumulation to the same level as AD patients [32, 33]. Interestingly, MCI subjects who at clinical follow-up converted to AD showed higher PIB retention than subjects with non-progressive MCI, indicating that neocortical PIB retention is a marker for the prediction of progression to AD in the MCI stage [34]. A PIB-PET study in a nondemented population revealed elevated cortical retention of PIB in four nondemented persons [35]. These nondemented PIB-positive cases additionally showed an abnormality in the concentration of Aβ1-42 in cerebrospinal fluid, suggesting the presence of SPs in the absence of cognitive impairment [36]. There was a strong relationship between impaired memory performance and PIB binding in the nondemented population [37]. These findings suggest that amyloid imaging may be sensitive enough for the detection of a preclinical AD state. However, one should be careful when assessing abnormalities in the distribution of PIB, because PIB retention is also observed in cerebral amyloid angiopathy [38, 39]. Amyloid imaging may be useful as a surrogate marker for monitoring brain amyloid deposition during anti-amyloid therapy. However, longitudinal PIB-PET evaluation indicated relatively stable PIB retention after 2 years of follow-up in AD patients, suggesting that brain amyloid deposition reflected by PIB retention reaches a plateau at the early clinical stages of AD [40]. Therefore, therapy that retards the synthesis of Aβ (e.g., β- and γ-secretase inhibitors) should be started before the retention of amyloid-imaging tracers reaches a plateau.
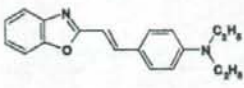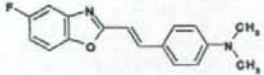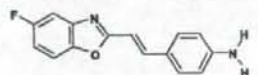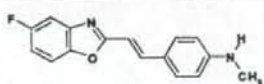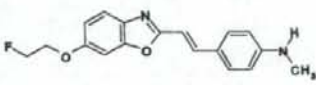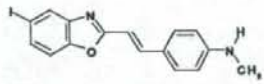
The stilbene derivative SB-13 has also been used in a human PET study [41]. In a PET study, [11C]SB-13 exhibited similar binding properties to PIB. For expanded use in clinical investigations, an 18F-labeled stilbene derivative is under investigation.

A PET study using [11C]BF-227 was performed at Tohoku University [23]. Neocortical retention of BF-227 was observed in an AD patient (Fig. (4)). A subject with MCI also showed cortical retention of BF-227. Interestingly, this subject was confirmed to progress to AD during the follow-up 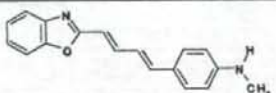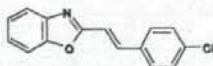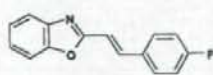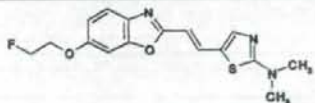period, suggesting that cortical retention of BF-227 indicates a high risk of conversion to AD in MCI subjects. Several MCI subjects showed a distribution of BF-227 similar to that in AD subjects. All Alzheimer's patients and about 60% of MCI subjects showed an elevated standardized uptake value (SUV) ratio in the neocortical regions. Even in MCI subjects showing prominent retention of BF-227, the neocortical SUV ratio was below the mean value observed in AD patients. This finding suggests that MCI is a pathologically transitional state between normal aging and dementia, and that the amyloid deposition reflected by BF-227 retention does not reach a plateau in the MCI stage. Voxel-by-voxel analysis of BF-227 PET images demonstrated higher retention of BF-227 in the temporoparietal region in AD patients [23]. The pattern of distribution resembles the distribution of neuritic plaques in postmortem AD brains [42, 43]. Microscopic observation also indicates preferential binding of BF-227 to neuritic plaques in AD brain sections (Fig. (3)). In an *in vitro* binding experiment, BF-227 binding to Aβ increased linearly with increasing Aβ fibril formation [24]. For these reasons, BF-227 is considered to bind neuritic plaques selectively *in vivo*. A validation study is required to determine whether the retention of BF-227 in the neocortex accurately reflects the level of neuritic plaques rather than the level of diffuse plaques.

FUTURE DIRECTION OF PROBE DEVELOPMENT

The commercialization of 18F-labeled agents or SPECT imaging agents is necessary for the wide clinical application of amyloid imaging. Because of the limited half-life of 11C (20 min), the supply of 11C-labeled PET agents is limited to facilities with an on-site cyclotron. 18F-labeled agents are generally easier for routine clinical use because of the longer half-life of 18F (110 min). Currently, several 18F-labeled agents for amyloid imaging are under clinical evaluation. To

Table 1. Binding Affinity of Benzoxazole Derivatives for Aβ Fibrils and Brain Uptakes After Intravenous Administration in Normal Mice

| Compounds	Chemical structure	Kd or Ki (nM)		Brain uptake (%ID/g)	
		Aβ1-40	Aβ1-42	2 min	30 min
BF-125		1.5 ± 0.76	4.9 ± 1.9	3.0 ± 0.87	3.0 ± 0.53
BF-133		2.1 ± 1.1	3.4 ± 0.73	5.5 ± 0.40	3.8 ± 0.030
BF-140		4.7 ± 2.2	2.1 ± 0.18	5.5 ± 0.60	1.1 ± 0.076
BF-145		3.0 ± 0.46	4.5 ± 1.9	4.4 ± 1.80	1.6 ± 0.40
BF-168		2.5 ± 2.3	6.4 ± 1.0	3.9 ± 0.22	1.6 ± 0.0071
BF-180		6.8 ± 1.4	10.6 ± 1.5	2.4 ± 0.52	1.8 ± 0.010
BF-185		2.5 ± 2.3	14 ± 10	3.9 ± 0.49	3.8 ± 0.16
BF-191		> 5000	> 5000	12 ± 0.26	1.7 ± 0.16
BF-208		> 5000	> 5000	5.6 ± 0.64	0.28 ± 0.024
BF-227		1.8 ± 0.42	4.3 ± 1.5	7.9 ± 0.18	0.54 ± 0.029
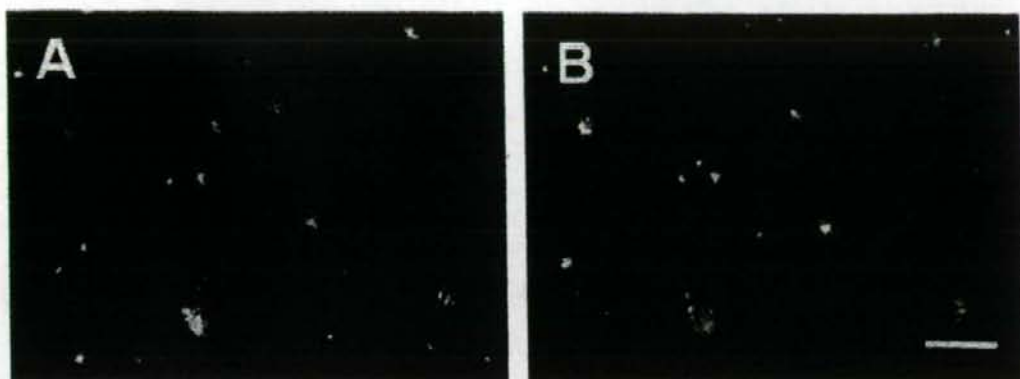
Fig. (3). Fluorescence microscopic images of senile plaques in Alzheimer's disease using BF-227 (A) and $A\beta$ specific antibody 6F/3D (B) Bar = 100μm.
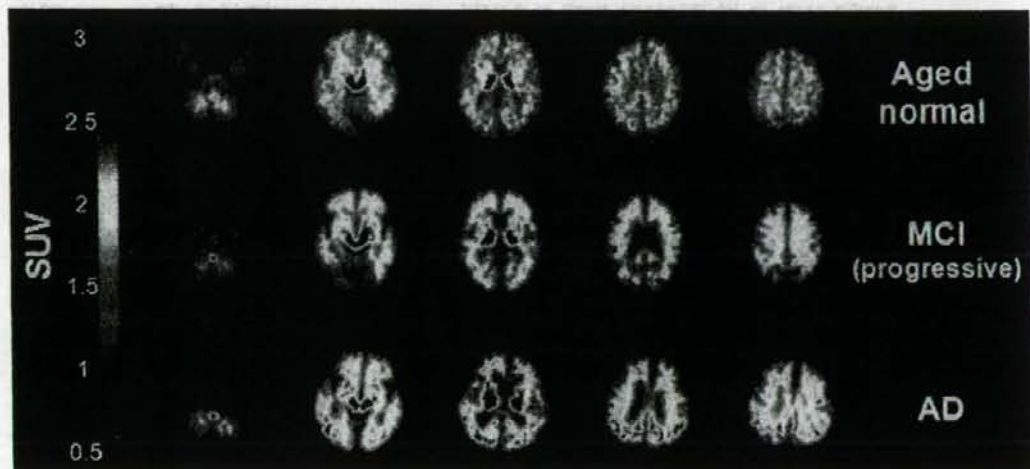

Fig. (4). Mean SUV images between 20 and 40 min post-injection of $[^{11}C]$BF-227 in aged normal, MCI and AD cases.

obtain a better understanding of the pathophysiology of AD, it is also necessary to visualize the distributions of $A\beta$ pathology and tau pathology individually. However, no surrogate markers are available for evaluating the deposition of NFTs in the brain, because of the difficulty in developing a tau-specific imaging probe [44]. We previously introduced the novel compounds BF-126 and BF-170 as candidates for tau imaging [45]. In AD brain sections, BF-126 and BF-170 visualize NFTs, neuropil threads, and PHF-type neuritis distinctly. For clinical application, optimization of these compounds to reduce non-specific binding is in progress.

CONCLUSION

Several amyloid-imaging agents have been successfully developed for PET imaging. These agents displayed high binding affinity for $A\beta$ fibrils and high BBB permeability. $[^{11}C]$PIB, $[^{18}F]$FDDNP, and $[^{11}C]$BF-227 displayed selective

in vivo binding to amyloid in the brain and clearly differentiated early AD patients from normal populations. The development of ^{18}F-labeled agents or SPECT imaging agents is necessary for the wide application of amyloid imaging. The development of an NFT-specific imaging agent is also much needed. Amyloid imaging is currently the best method for the early and accurate diagnosis of AD and for monitoring amyloid pathology in the brain. This imaging technology and the forthcoming anti-amyloid therapy will cooperatively contribute to the prevention of dementia.

ACKNOWLEDGEMENTS

Program of the New Energy and Industrial Technology Development Organization (NEDO) of Japan, Health and Labour Sciences Research Grants for Translational Research from the Japanese Ministry of Health, Labour and Welfare, and a JST grant for research and education in molecular imaging.

DISCLOSURE STATEMENT

All authors have no conflict of interest.

REFERENCES

[1]   Tanzi RB, Bertram L. Twenty years of the Alzheimer's disease amyloid hypothesis: a genetic perspective. Cell 2005; 120: 545-555.

[2]   Goldman WP, Price JL, Storandt M, et al. Absence of cognitive impairment or decline in preclinical Alzheimer's disease. Neurology 2001; 56: 361-367.

[3]   Price JL, Morris JC. Tangles and plaques in nondemented aging and "preclinical" Alzheimer's disease. Ann Neurol 1999; 45: 358-368.

[4]   Klunk WE, Debnath ML, Pettegrew JW. Development of small molecule probes for the beta-amyloid protein of Alzheimer's disease. Neurobiol Aging 1994; 691-698.

[5]   Klunk WE, Debnath ML, Pettegrew JW. Chrysamine-G binding to Alzheimer and control brain: autopsy study of a new amyloid probe. Neurobiol Aging 1995; 16: 541-548.

[6]   Skovronsky DM, Zhang B, Kung MP, Kung HF, Trojanowski JQ, Lee VM. In vivo detection of amyloid plaques in a mouse model of Alzheimer's disease. Proc Natl Acad Sci USA 2000; 97: 7609-7614.

[7]   Zhuang ZP, Kung MP, Hou C, et al. Radioiodinated styrylbenzenes and thioflavins as probes for amyloid aggregates. J Med Chem 2001; 44: 1905-1914.

[8]   Klunk WE, Bacskai BJ, Mathis CA, et al. Imaging Abeta plaques in living transgenic mice with multiphoton microscopy and methoxy-X04, a systemically administered Congo red derivative. J Neuropathol Exp Neurol 2002; 61: 797-805.

[9]   Shoghi-Jadid K, Small GW, Agdeppa ED, et al. Localization of neurofibrillary tangles and beta-amyloid plaques in living patients with Alzheimer disease. Am J Geriatr Psychiatry 2002; 10: 24-35.

[10]   Agdeppa ED, Kepe V, Liu J, et al. Binding characteristics of radiofluorinated 6-dialkylamino-2-naphthylethylidene derivatives as positron emission tomography imaging probes for beta-amyloid plaques in Alzheimer's disease. J Neurosci 2001; 21: RC189.

[11]   Agdeppa ED, Kepe V, Petri A, et al. In vitro detection of (S)-naproxen and ibuprofen binding to plaques in the Alzheimer's brain using the positron emission tomography molecular imaging probe 2-(1-[6-[(2-[(18)F]fluoroethyl)(methyl) amino]-2-naphthyl]ethyl-idene)malononitrile. Neuroscience 2003; 117: 723-730.

[12]   Mathis CA, Wang Y, Klunk WE. Imaging beta-amyloid plaques and neurofibrillary tangles in the aging human brain. Curr Pharm Des 2004; 10: 1469-1492.

[13]   Klunk WE, Wang Y, Huang GF, Debnath ML, Holt DP, Mathis CA. Uncharged thioflavin-T derivatives bind to amyloid-beta protein with high affinity and readily enter the brain. Life Sci 2001; 69: 1471-1484.

[14]   Klunk WE, Wang Y, Huang GF, et al. The binding of 2-(4'-methylaminophenyl)benzothiazole to postmortem brain homoge-nates is dominated by the amyloid component. J Neurosci 2003; 23: 2086-2092.

[15]   Kung MP, Hou C, Zhuang ZP, et al. IMPY: an improved thioflavin-T derivative for in vivo labeling of beta-amyloid plaques. Brain Res 2002; 956: 202-210.

[16]   Kung HF, Kung MP, Zhuang ZP, et al. Iodinated tracers for imaging amyloid plaques in the brain. Mol Imaging Biol 2003; 5: 418-426.

[17]   Ono M, Wilson A, Nobrega J, et al. ^{11}C-labeled stilbene derivatives as Abeta-aggregate-specific PET imaging agents for Alzheimer's disease. Nucl Med Biol 2003; 30: 565-571.

[18]   Ono M, Kawashima H, Nonaka A, et al. Novel benzofuran derivatives for PET imaging of beta-amyloid plaques in Alzheimer's disease brains. J Med Chem 2006; 49: 2725-2730.

[19]   Suemoto T, Okamura N, Shiomitsu T, et al. In vivo labeling of amyloid with BF-108. Neurosci Res 2004; 48: 65-74.

[20]   Okamura N, Suemoto T, Shimadzu H, et al. Styrylbenzoxazole derivatives for in vivo imaging of amyloid plaques in the brain. J Neurosci 2004; 24: 2535-2541.

[21]   Okamura N, Suemoto T, Shiomitsu T, et al. A novel imaging probe for in vivo detection of neuritic and diffuse amyloid plaques in the brain. J Mol Neurosci 2004; 24: 247-255.

[22]   Furumoto S, Okamura N, Iwata R, Yanai K, Arai H, Kudo Y. Recent advances in the development of amyloid imaging agents. Curr Top Med Chem 2007; 7: 1773-1789.

[23]   Kudo Y, Okamura N, Furumoto S, et al. 2-(2-[2-Dimethyl-aminothiazol-5-yl]ethenyl)-6- (2-[fluoro]ethoxy)benzoxazole: a novel PET agent for in vivo detection of dense amyloid plaques in Alzheimer's disease patients. J Nucl Med 2007; 48: 553-561.

[24]   Okamura N, Furumoto S, Funaki Y, et al. Binding and safety profile of novel benzoxazole derivative for in vivo imaging of amyloid deposits in Alzheimer's disease. Geriatr Gerontol Int 2007 (in press)

[25]   Small GW, Kepe V, Ercoli LM, et al. PET of brain amyloid and tau in mild cognitive impairment. N Engl J Med 2006; 355: 2652-2663.

[26]   Petersen RC, Parisi JE, Dickson DW, et al. Neuropathologic features of amnestic mild cognitive impairment. Arch Neurol 2006; 63: 665-672.

[27]   Boxer AL, Rabinovici GD, Kepe V, et al. Amyloid imaging in distinguishing atypical prion disease from Alzheimer disease. Neurology 2007; 69: 283-290.

[28]   Bacskai BJ, Klunk WE, Mathis CA, Hyman BT. Imaging amyloid-beta deposits in vivo. J Cereb Blood Flow Metab 2002; 22: 1035-1041.

[29]   Klunk WE, Engler H, Nordberg A, et al. Imaging brain amyloid in Alzheimer's disease with Pittsburgh Compound-B. Ann Neurol 2004; 55: 306-319.

[30]   Price JC, Klunk WE, Lopresti BJ, et al. Kinetic modeling of amyloid binding in humans using PET imaging and Pittsburgh Compound-B. J Cereb Blood Flow Metab 2005; 25: 1528-1547.

[31]   Lopresti BJ, Klunk WE, Mathis CA, et al. Simplified quantification of Pittsburgh Compound B amyloid imaging PET studies: a comparative analysis. J Nucl Med 2005; 46: 1959-1972.

[32]   Rowe CC, Ng S, Ackermann U, et al. Imaging beta-amyloid burden in aging and dementia. Neurology. 2007; 68: 1718-1725.

[33]   Kemppainen NM, Aalto S, Wilson IA, et al. PET amyloid ligand [11C]PIB uptake is increased in mild cognitive impairment. Neurology 2007; 68: 1603-1606.

[34]   Forsberg A, Engler H, Almkvist O, et al. PET imaging of amyloid deposition in patients with mild cognitive impairment. Neurobiol Aging 2007 (in press)

[35]   Mintun MA, Larossa GN, Sheline YI, et al. [11C]PIB in a nondemented population: potential antecedent marker of Alzheimer's disease. Neurology 2006; 67: 446-452.

[36]   Fagan AM, Mintun MA, Mach RH, et al. Inverse relation between in vivo amyloid imaging load and cerebrospinal fluid Abeta42 humans. Ann Neurol 2006; 59: 512-519.

[37]   Pike KE, Savage G, Villemagne VL, et al. Beta-amyloid imaging and memory in non-demented individuals: evidence for preclinical Alzheimer's disease. Brain 2007; 130: 2837-2844.

[38]   Bacskai BJ, Frosch MP, Freeman SH, et al. Molecular imaging with Pittsburgh Compound B confirmed at autopsy: a case report. Arch Neurol 2007; 64: 431-434.

[39]   Johnson KA, Gregas M, Becker JA, et al. Imaging of amyloid burden and distribution in cerebral amyloid angiopathy. Ann Neurol 2007; 62: 229-234.

[40]   Engler H, Forsberg A, Almkvist O, et al. Two-year follow-up of amyloid deposition in patients with Alzheimer's disease. Brain 2006; 129: 2856-2866.

[41]   Verhoeff NP, Wilson AA, Takeshita S, et al. In-vivo imaging of Alzheimer disease beta-amyloid with [11C]SB-13 PET. Am J Geriatr Psychiatry 2004; 12: 584-595.

[42]   Arnold SE, Hyman BT, Flory J, Damasio AR, Van Hoesen GW. The topographical and neuroanatomical distribution of neuro-fibrillary tangles and neuritic plaques in the cerebral cortex of patients with Alzheimer's disease. Cereb Cortex 1991; 1: 103-116.

[43]   Cummings JL, Cole G. Alzheimer disease. JAMA 2002; 287: 2335-2338.

[44]   Small GW, Agdeppa ED, Kepe V, Satyamurthy N, Huang SC, Barrio JR. *In vivo* brain imaging of tangle burden in humans. J Mol Neurosci 2002; 19: 323-327.

[45]   Okamura N, Suemoto T, Furumoto S, *et al.* Quinoline and benzimidazole derivatives: candidate probes for *in vivo* imaging of tau pathology in Alzheimer's disease. J Neurosci 2005; 25: 10857-10862.

Elevated Cerebrospinal Fluid Tau Protein Levels in Wernicke's Encephalopathy

Sachio Matsushita, Tomohiro Miyakawa, Hitoshi Maesato, Toshifumi Matsui,
Akira Yokoyama, Hiroyuki Arai, Susumu Higuchi, and Haruo Kashima

Objective: Limited neuronal cell loss is seen in the neuropathology of Wernicke's encephalopathy (WE), but the extent of neuronal damage has not been well studied. Moreover, there is still a debate as to whether alcohol itself causes brain damage in humans. Although, it is difficult to examine the extent of neuronal damage in living patients, recent studies have revealed that total tau protein levels in the cerebrospinal fluid (CSF) reflect the rate of neuronal degeneration. Therefore, we hypothesized that the elevated CSF total tau in patients with WE was due to neuronal damage and thus we examined CSF total tau protein in patients with WE, as well as in those with alcohol withdrawal delirium (WD) and Korsakoff syndrome (KS). We also examined CSF total tau in nonalcohol dependent patients with Alzheimer's disease (AD) as a disease control.

Methods: CSF samples were obtained from 13 acute WE patients with alcohol dependence, 9 WD patients with alcohol dependence and 16 KS patients with alcohol dependence, and from 20 nonalcohol dependent AD patients. CSF was also obtained from 10 of the WE patients after their disease had progressed to the chronic stage. CSF tau protein levels in all samples were determined by sandwich enzyme-linked immunosorbent assay. Tau phosphorylated at threonine 181 (p-tau$_{181}$) and amyloid β-protein ending at amino acid 42 (Aβ42) in CSF were also determined for comparison between acute WE with AD.

Results: Total tau was significantly elevated in acute WE and decreased on long-term follow-up, but was not elevated in WD or KS. The patterns of p-tau$_{181}$ and Aβ42 differed between acute WE and AD.

Conclusions: Intense neuronal cell death occurs transiently in WE, and the mechanism differs from that in AD. Neuronal damage is generally unaccompanied in WD. These results suggest that CSF total tau is a useful biological marker for WE.

Key Words: Cerebrospinal Fluid, Tau Protein, Wernicke's Encephalopathy, Korsakoff Syndrome, Alcohol Withdrawal Delirium.

WERNICKE 's encephalopathy (WE), a serious neurological disorder that results from thiamine deficiency, is encountered in alcohol dependence and in patients with grossly impaired nutritional status, and is often followed by Korsakoff syndrome (KS). In WE neuropathology, loss of neurons is the most consistent abnormality in structures such as the thalamus and cerebellar vermis (Hazell et al., 1998). The brain shrinkage seen in WE has been attributed to the loss of both axons and neurons in the cerebral cortex (Kril et al., 1997).

Neuronal cell death in WE is complex and not fully understood. Several mechanisms have been proposed, including decreases in the activity of a thiamine-requiring enzyme, the α-ketoglutarate dehydrogenase complex (Butterworth and Héroux, 1989), decreases in energy production due to a reduction in ATP content (Aikawa et al., 1984), accumulation of lactate and resulting pH changes in the brain (Hakim, 1984), and increased extracellular glutamate concentrations (Hazell et al., 1993).

In animal studies, binge drinking has been reported to produce neurodegeneration in corticolimbic areas (Collins et al., 1996) and ethanol withdrawal has been reported to induce hippocampal cytotoxicity (Prendergast et al., 2000). There is still debate, however, as to whether alcohol itself causes brain damage in humans (Harper, 1998). For example, Kril et al. (1997) reported selective neuronal loss in the superior frontal association cortex of chronic alcoholics, while another study reported no significant differences between the numbers of neocortical neurons in controls and alcoholics (Jensen and Pakkenberg, 1993).

As a fingerprint of neuropathology, total tau protein in the cerebrospinal fluid (CSF) has been intensively studied. According to a recent study, total tau probably reflects the

rate of neuronal degeneration in chronic neurodegenerative disorders (Blennow and Hampel, 2003). In fact, an increase in CSF total tau is reported to be a useful biological diagnostic marker for Alzheimer's disease (AD) (Arai et al., 1995; Blennow and Hampel, 2003), but our previous examination of CSF total tau in KS showed it to be in the normal range (Morikawa et al., 1999).

We hypothesized that total tau in CSF may be a useful indicator of the extent of neuronal cell death in WE, as well as in severe alcohol withdrawal states, and that it would have diagnostic utility as a biological marker for WE. Thus, we designed this study to examine the temporal profiles of total tau in WE. We also examined CSF total tau in cases of alcohol withdrawal delirium (WD), which is often difficult to differentiate from WE, and in KS. Finally, we extended our study beyond total tau to determine the levels of tau phosphorylated at threonine 181 (p-tau$_{181}$) and of amyloid β-protein ending at amino acid 42 (Aβ42) in the CSF of patients with WE for comparison with the levels found in the CSF of AD patients.

Amyloid β protein (Aβ) is the major constituent of the senile plaques typical in AD and a decrease in CSF Aβ42 in patients with AD has been consistently reported (Formichi et al., 2006). Although a reduction in CSF Aβ42 in AD has been postulated to reflect deposition of peptide Aβ in senile plaques, and the resulting decrease in levels of diffusion into the CSF (Formichi et al., 2006), other possible causes, such as axonal degeneration (Sjögren et al., 2002) or entrapment in narrow interstitial and subarachnoid drainage pathways (Sjögren et al., 2001), have been proposed.

Phosphorylated tau protein is reported to be the main component of the paired helical filaments (PHF) that contribute to the formation of neurofibril tangles (NFT), which comprise a compact filamentous network found mainly in the hippocampus, entorhinal cortex, and amygdala cells of the AD brain (Formichi et al., 2006). In AD, elevated levels of phosphorylated tau protein in the CSF have been reported. However, because there are no changes in the concentration of phosphorylated tau protein after acute stroke (Hesse et al., 2001), or in Creutzfeldt-Jakob disease (Riemenschneider et al., 2003), the concentration of phosphorylated tau protein

in the CSF is not a marker for neuronal damage, but rather specifically reflects the phosphorylation state of tau protein (Blennow and Hampel, 2003). Therefore, we hypothesized that by examining CSF p-tau$_{181}$ and Aβ42, we could obtain insight into the mechanisms of neuronal damage in WE.

METHODS

Subjects

The Ethics Committee of the National Hospital Organization, Kurihama Alcoholism Center approved this study, and all participants or their families gave informed consent. All subjects, except for the AD patients were alcohol-dependent. Subjects included 13 male alcohol dependent patients (mean age ± standard deviation, 58.5 ± 9.3 years) diagnosed with WE and consecutively admitted to the Kurihama Alcoholism Center. All met the Diagnostic and Statistical Manual of Mental Disorders, 4th edition (DSM-IV) criteria for diagnosis of alcohol dependence (American Psychiatric Association, 1994). The diagnosis of WE was made based on clinical features, and all of patients met the operational criteria for diagnosis of WE (Caine et al., 1997), as shown in Table 1. After drawing blood samples to determine thiamine levels, we treated all WE patients with intravenous thiamine, 100 mg/d for 7 to 15 days.

Diagnosis of WD in 9 male alcohol dependent patients (aged 56.3 ± 7.5 years) and of KS in 16 male alcohol-dependent patients (aged 55.5 ± 6.1 years) at the Kurihama Alcoholism Center were based on DSM-IV criteria (American Psychiatric Association, 1994). KS included patients who had been diagnosed as having KS and lacked WE symptoms at the time of lumbar puncture. Non-alcohol dependent probable AD was diagnosed at the Kurihama Alcoholism Center using the NINCDS-ADRDA criteria (McKhann et al., 1984) for the group of 20 AD patients (11 men and 9 women, aged 72.0 ± 10.3 years) included in the study.

CSF Tau Protein Measurement

CSF was collected from each subject by routine lumbar puncture under informed consent from the patients and/or their families. In WE patients, baseline lumbar puncture was performed while at least one of the WE triad symptoms existed (i.e., during acute WE). In the case of WD patients, lumbar puncture was performed in the presence of delirium.

Routine CSF examination, including total protein content, glucose levels and CSF pressure, confirmed normal ranges for all values in acute WE patients. CSF samples were centrifuged at 1500 rpm (430 × g) for 10 minutes at 4°C, and the supernatants were aliquoted and kept at −80°C until analysis. Total tau, p-tau$_{181}$ and Aβ42 levels in the CSF were determined by a sensitive sandwich enzyme-linked

Table 1. Clinical Symptoms of 13 Patients During the Acute Stage of Wernicke's Encephalopathy

Patient number	1	2	3	4	5	6	7	8	9	10	11	12	13
Age at admission (years)	67	67	64	63	51	67	61	62	46	62	54	47	38
Days between onset of WE and lumbar puncture	13	35	36	28	12	9	5	44	9	13	7	16	30
BMI at admission	19.6	19.1	20.9	16.5	21.1	22.0	NA	16.7	18.4	19.0	NA	16.2	17.6
Serum thiamine levels (ng/ml)	48.8	38.2	20.9	34.3	27.8	20.8	17.2	NA	7.4	12.2	NA	15.7	NA
Ophthalmoplegia	−	−	−	−	−	+	+	+	+	+	+	+	−
Nystagmus	+	+	−	−	−	−	−	+	+	−	+	−
Ataxia	+	+	+	+	−	+	+	+	+	+	+	+	−
Altered mental state	+	+	+	+	+	+	+	+	+	+	+	+	+
Severe amnesia	+	+	+	+	+	+	+	+	+	+	+	+	+
MMSE scores after treatment	28	NA	21	15	25	28	29	22	24	20	19	28	30
1st CSF total tau level (pg/ml)	1827	732	1108	1308	385	1048	912	875	554	929	1995	363	1755
2nd CSF total tau level (pg/ml)	142	128	247	51	260	147	149	113	282	217	NA	NA	NA

NA, not available; WE, Wernicke's encephalopathy; CSF, cerebrospinal fluid; MMSE, Mini-Mental State Examination.

immunosorbent assay (ELISA, Innogenetics, Ghent, Belgium) according to the manufacturer's instructions. CSF total tau ≤ 200 pg/ml was considered normal; total tau ≥ 400 pg/ml was considered abnormal.

With the additional informed consent of each patient and/or family, we performed follow-up lumbar puncture for analysis of CSF tau in 10 of the 13 WE patients during the chronic stage of the disease. We could not perform follow-up in 3 WE patients because 2 had been discharged and 1 did not consent. For this study, we defined the chronic stage as the state in which all WE symptoms except amnesia had vanished. We administered the Mini-Mental State Examination (MMSE) (Folstein et al., 1975) during the chronic stage of WE. The mean duration between baseline lumbar puncture and follow-up lumbar puncture was 169.1 ± 59.8 days (range; 88 to 272 days).

Statistical Analyses

Statistical calculations were preformed using an SAS package (Statistical Analysis System; SAS Institute, Inc., Cary, NC). Continuous variables were compared by Student's t-test or ANOVA. Probability differences with p-values of less than 0.05 were considered statistically significant.

RESULTS

Mean total tau levels in CSF were 1060.9 ± 531.3 pg/ml in acute WE, 157.1 ± 92.4 pg/ml in WD, 137.4 ± 59.9 pg/ml in KS, and 704.9 ± 400.9 pg/ml in AD (Fig. 1). Total tau neither correlated with clinical severity (number of WE symptoms) nor reflected the scores from MMSE performed during the chronic stage. One-way ANOVA for individual comparison of total tau in acute WE with total tau in WD, KS and chronic WE showed that in the patients with acute WE, total tau was significantly higher ($p < 0.0001$) than in groups of alcohol-dependent patients with other diagnoses. CSF total tau levels in acute WE were also significantly higher than those in AD ($p = 0.036$). On follow-up, we found that in all 10 WE patients' reassessed, total CSF tau levels in the chronic stage of WE had declined from baseline (Fig. 2) to a mean of 173.6 ± 74.2 pg/ml.
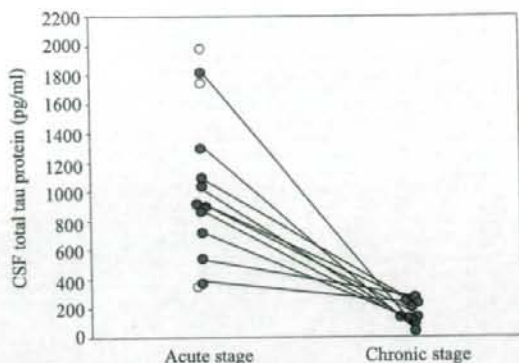

Fig. 2. Changes in CSF total tau levels as acute Wernicke's encephalopathy progressed to chronic WE (mean follow-up time, 169.1 ± 59.8 days). Patients with acute WE who did not undergo follow-up lumbar puncture for evaluation of CSF total tau during chronic WE are represented by open circles.

Mean p-tau$_{181}$ levels in the CSF of the 20 AD patients (71.8 ± 25.2 pg/ml; range, 33 to 119 pg/ml) was significantly higher than the 32.1 ± 11.3 pg/ml (range, 18 to 54 pg/ml) found in patients with acute WE ($p < 0.0001$; Fig. 3). In contrast, Aβ42 was significantly higher in acute WE than in AD: 646.1 ± 244.2 pg/ml versus 395.2 ± 156.2 pg/ml, ranging from 317 to 1037 pg/ml in acute WE and from 222 to 797 pg/ml in AD ($p = 0.0013$; Fig. 4).

DISCUSSION

In this study, we found that: (1) total tau levels in CSF were elevated in acute WE, but had declined at follow-up; (2) CSF p-tau$_{181}$ levels were lower in acute WE than in AD, while Aβ42 levels were higher in acute WE than in AD; and (3) total tau was not elevated in WD or in KS. These results
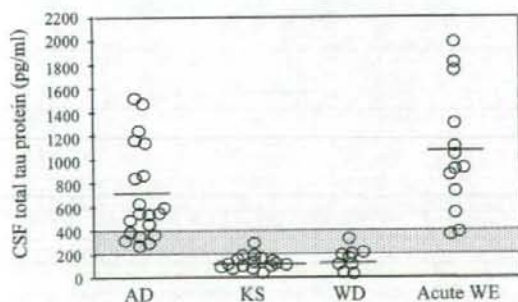

Fig. 1. CSF total tau levels in subjects with Alzheimer's disease ($n = 20$), Korsakoff syndrome ($n = 16$), alcohol withdrawal delirium ($n = 9$), and acute Wernicke's encephalopathy ($n = 13$). Highlighted band indicates borderline levels of total tau for a particular diagnosis. Horizontal bars indicate mean levels of total tau for each diagnostic group. AD, Alzheimer's disease; KS, Korsakoff syndrome; WD, alcohol withdrawal delirium; WE, Wernicke's encephalopathy.
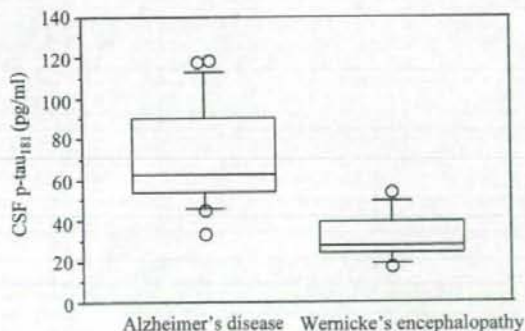

Fig. 3. CSF p-tau$_{181}$ levels in acute Wernicke's encephalopathy and Alzheimer's disease. The horizontal lines within the boxes indicate median values, and the upper and lower hinges of the boxes indicate the 75th and 25th percentiles, respectively. The limit lines depict range; outliers are represented by open circles. AD, Alzheimer's disease; WE, Wernicke's encephalopathy.
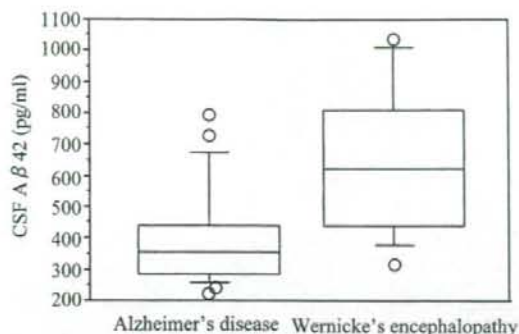
Fig. 4. CSF Aβ42 levels in acute Wernicke's encephalopathy and Alzheimer's disease. The horizontal lines within boxes indicate median values and the upper and lower hinges of the boxes indicate the 75th and 25th percentiles, respectively. The limit lines depict range; outliers are represented by open circles.

strongly suggest that extensive neuronal cell death occurred transiently in WE. As described above, CSF p-tau$_{181}$ increases and CSF Aβ42 decreases in patients with AD. Therefore, lower levels of CSF p-tau$_{181}$ and higher levels of CSF Aβ42 in WE than in AD suggest that the mechanisms of neuronal death differ between WE and AD. Moreover, the decline in total tau from the high levels found in acute WE coupled with the finding of normal levels of total tau in chronic WE, suggest that neuronal death is transient, not progressive, in WE. Transiently elevated CSF total tau and nonelevated CSF phospho-tau also characterize acute stroke (Hesse et al., 2001). These findings clearly suggest common mechanisms for CSF total tau elevation, i.e., extensive neuronal cell loss, in WE and acute stroke.

Our study indicates that in WD, neuronal cell death does not occur, or that the extent of neuronal damage is much less severe than in WE. Our WD subjects had normal total tau levels, with the exception of one case of borderline elevated total tau. On the other hand, our results demonstrate the potential clinical importance of CSF total tau levels as a biological marker of WE and KS. Although a diagnosis of WE can be made by the classic clinical triad of oculomotor abnormalities, gait ataxia and a global confusional state, the fact that two-thirds of patients with WE do not present the classic clinical triad (Victor et al., 1989) indicates that WE is difficult to diagnose during life. Thus, it is often difficult to distinguish WE from WD (Hersh et al., 1997). Most clinicians differentiate these clinical entities based on only patient symptoms and their response to thiamine administration, but a more accurate method of diagnosis is needed because of the frequently poor prognosis of patients with WE. Recent magnetic resonance imaging (MRI) results (Antunez et al., 1998) notwithstanding, the sensitivity and specificity of MRI diagnosis remains to be established as a clinically useful ante mortem diagnostic technique for WE (Antunez et al., 1998).

In KS patients, both memory disturbance and global cognitive impairment are frequent complications. The initial clinical manifestations of KS vary from acute coma to insidious onset of memory impairment. A history of WE is not invariably present in cases of KS (Kopelman, 1995). Similarly, differentiating KS from AD is frequently difficult, but early diagnosis of AD is needed to initiate symptomatic treatment with acetylcholinesterase inhibitors.

Our study has some limitations, including the small sample size and a lack of normal control subjects. However, CSF total tau has been intensively studied and according to recent review of CSF markers for AD, 36 different studies have used similar methods as our study, and these studies have included 2500 AD patients and 1400 controls (Blennow and Hampel, 2003). Therefore, we believe that a normal range for CSF total-tau level has been established.

In conclusion, this is the first study to describe the transient elevation of total tau levels in CSF of patients with WE, as well as the absence of elevated total tau in WD. These preliminary results remain to be confirmed in larger samples and to be extended in future investigations of autopsy-confirmed cases of WE.

ACKNOWLEDGMENTS

COMPETING INTERESTS

None.

REFERENCES

Aikawa H, Watanabe IS, Furuse T, Iwasaki Y, Satoyoshi E, Sumi T, Moroji T (1984) Low energy levels in thiamine-deficient encephalopathy. J Neuropathol Exp Neurol 43:276–287.

American Psychiatric Association (1994) Diagnostic and Statistical Manual of Mental Disorders, 4th ed. American Psychiatric Press, Washington, DC.

Antunez E, Estruch R, Cardenal C, Nicolas JM, Fernandez-Sola J, Urbano-Marquez A (1998) Usefulness of CT and MRI imaging in the diagnosis of acute Wernicke's encephalopathy. AJR Am J Roentgenol 171:1131–1137.

Arai H, Terajima M, Miura M, Higuchi S, Muramatsu T, Machida N, Seiki H, Takase S, Clark CM, Lee VM-Y, Trojanowski JQ, Sasaki H (1995) Tau in cerebrospinal fluid: a potential diagnostic marker in Alzheimer's disease. Ann Neurol 38:649–652.

Blennow K, Hampel H (2003) CSF markers for incipient Alzheimer's disease. Lancet Neurol 2:605–613.

Butterworth RF, Héroux M (1989) Effect of pyrithiamine treatment and subsequent thiamine rehabilitation on regional cerebral amino acids and thiamine-dependent enzymes. J Neurochem 52:1079–1084.

Caine D, Halliday GM, Kril JJ, Harper CG (1997) Operational criteria for the classification of chronic alcoholics: identification of Wernicke's encephalopathy. J Neurol Neurosurg Psychiatry 62:51–60.

Collins MA, Corso TD, Neafsey EJ (1996) Neuronal degeneration in rat cerebrocortical and olfactory regions during subchronic "binge" intoxication with ethanol: possible explanation for olfactory deficits in alcoholics. Alcohol Clin Exp Res 20:284–292.

Folstein MF, Folstein SE, McHugh PR (1975) "Mini-mental state." A practical method for grading the cognitive state of patients for the clinicians. J Psychiatr Res 12:189–198.

Formichi P, Battisti C, Radi E, Federico A (2006) Cerebrospinal fluid tau, $A\beta$, and phosphorylated tau protein for the diagnosis of Alzheimer's disease. J Cell Physiol 208:39–46.

Hakim AM (1984) The induction and reversibility of cerebral acidosis in thiamine deficiency. Ann Neurol 16:673–679.

Harper C (1998) The neuropathology of alcohol-specific brain damage, or does alcohol damage brain? J Neuropathol Exp Neurol 57:101–110.

Hazell AS, Butterworth RF, Hakim AM (1993) Cerebral vulnerability is associated with selective increase in extracellular glutamate concentration in experimental thiamine deficiency. J Neurochem 61:1155–1158.

Hazell AS, Todd KG, Butterworth RF (1998) Mechanisms of neuronal cell death in Wernicke's encephalopathy. Metab Brain Dis 13:97–122.

Hersh D, Kranzler HR, Meyer RE (1997) Persistent delirium following cessation of heavy alcohol consumption: diagnostic and treatment implications. Am J Psychiatry 154:846–851.

Hesse C, Rosengren L, Andreasen N, Davidsson P, Vanderstichele H, Vanmechelen E, Blennow K (2001) Transient increase in total tau but not phosphor-tau in human cerebrospinal fluid after acute stroke. Neurosci Lett 297:187–190.

Jensen GB, Pakkenberg B (1993) Do alcoholics drink their neurons away? Lancet 342:1201–1204.

Kopelman MD (1995) The Korsakoff syndrome. Br J Psychiatry 166:154–173.

Kril JJ, Halliday GM, Svoboda MD, Cartwright H (1997) The cerebral cortex is damaged in chronic alcoholics. Neuroscience 79:983–998.

McKhann G, Drachman D, Folstein M, Katzman R, Price D, Stadlan EM (1984) Clinical diagnosis of Alzheimer's disease: report of the NINCDS-ADRDA Work Group under the auspices of Department of Health and Human Services Task Force on Alzheimer's Disease. Neurology 34:939–944.

Morikawa Y, Arai H, Matsushita S, Kato M, Higuchi S, Miura M, Kawakami H, Higuchi M, Okamura N, Tashiro M, Matsui T, Sasaki H (1999) Cerebrospinal fluid tau protein levels in demented and nondemented alcoholics. Alcohol Clin Exp Res 23:575–577.

Prendergast MA, Harris BR, Blanchard JA, Mayer S, Gibson DA, Littleton JM (2000) In vitro effects of ethanol withdrawal and spermidine on viability of hippocampus from male and female rat. Alcohol Clin Exp Res 24:1855–1861.

Riemenschneider M, Wagenpfeil S, Vanderstichele H, Otto M, Wiltfang J, Kretzschmar H, Vanmechelen E, Förstl H, Kurz A (2003) Phospho-tau/total tau ratio in cerebrospinal fluid discriminates Creutzfeldt-Jakob disease from other dementias. Mol Psychiatry 8:343–347.

Sjögren M, Davidsson P, Wallin A, Granerus AK, Grundstrom E, Askmark H, Vanmechelen E, Blennow K (2002) Decreased CSF-β-amyloid 42 in Alzheimer's disease and amyotropic lateral sclerosis may reflect mismetabolism of β-amyloid induced by separate mechanisms. Dement Geriatr Cogn Disord 13:1112–1118.

Sjögren M, Gisslen M, Vanmechelen E, Blennow K (2001) Low cerebrospinal fluid beta-amyloid 42 in patients with acute bacterial meningitis and normalization after treatment. Neurosci Lett 314:33–36.

Victor M, Adams RA, Collins GH (1989) The Wernicke-Korsakoff Syndrome and Related Disorders Due to Alcoholism and Malnutrition. F.A. Davis Co, Philadelphia.

In vivo visualization of donepezil binding in the brain of patients with Alzheimer's disease

Nobuyuki Okamura,[1] Yoshihito Funaki,[2] Manabu Tashiro,[3]
Motohisa Kato,[1] Yoichi Ishikawa,[2] Masahiro Maruyama,[4]
Hiroyasu Ishikawa,[5] Kenichi Meguro,[5] Ren Iwata[2] & Kazuhiko Yanai[1]

[1]*Department of Pharmacology, Tohoku University Graduate School of Medicine, Sendai,* [2]*Division of
Radiopharmaceutical Chemistry, Cyclotron and Radioisotope Center, Tohoku University, Sendai,*
[3]*Division of Nuclear Medicine, Cyclotron and radioisotope centre, Tohoku University, Sendai,*
[4]*Department of Geriatric and Complementary Medicine, Tohoku University Graduate School of
Medicine, Sendai and* [5]*Department of Geriatric Behavioural Neurology, Tohoku University Graduate
School of Medicine, Sendai, Japan*

WHAT IS ALREADY KNOWN ABOUT THIS SUBJECT

WHAT THIS STUDY ADDS

AIMS
The aims of this study were to visualize *in vivo* binding of donepezil to
acetylcholinesterase (AChE) in the brain and to establish a method for
measuring the amount of binding of orally administered donepezil.

METHODS
[5-^{11}C-methoxy]-donepezil ([^{11}C]-donepezil) was radiolabelled as a
positron emission tomography (PET) tracer. The biodistribution of
[^{11}C]-donepezil was measured by PET in 10 AD patients and six elderly
normal subjects. Two AD patients underwent additional PET
measurements after oral administration of donepezil for 6 months.

RESULTS
[^{11}C]-donepezil-PET images demonstrated high densities of tracer
distribution in AChE-rich brain regions such as the striatum, thalamus,
and cerebellum. Compared with elderly normal subjects, patients with
mild AD exhibited about 18–20% reduction of donepezil binding in the
neocortex and hippocampus, while patients with moderate AD
exhibited about 24–30% reduction of donepezil binding throughout
the brain. Orally administered donepezil (5 mg day^{-1}) induced
61.6–63.3% reduction of donepezil binding in AD brains. The
distribution volume of [^{11}C]-donepezil in the hippocampus was
significantly correlated with MMSE scores in AD patients.

CONCLUSIONS
[^{11}C]-donepezil-PET enables quantitative measurement of donepezil
binding in the brain. AD patients exhibited reduction of donepezil
binding in the brain, even in the early stage of disease. Longitudinal
evaluation by this technique enables determination of AChE binding
occupancy of orally administered donepezil.

Introduction

Cholinergic deficit is consistently found in the brain of patients with Alzheimer's disease (AD). Reduction in the activity of choline acetyltransferase (ChAT) and acetylcholinesterase (AChE) is evident in AD brains and correlates with cognitive decline [1, 2]. For this reason, cholinergic enhancement is a major approach to the treatment of AD. Currently, several AChE inhibitors (AChEIs) are widely prescribed to improve cognitive function in patients with AD [3]. However, not all patients respond to these treatments. It is thus important to identify factors that determine individual responses to treatment with AChEIs.

Functional imaging of cholinergic function is a useful strategy for determination of the treatment protocol of demented patients. Use of AChEIs themselves as radiotracers enables direct investigation of the pharmacokinetics of AChEIs using positron emission tomography (PET). Donepezil hydrochloride is currently the AChEI most widely used for the treatment of AD. It exhibits selective binding of AChE compared with butyrylcholinesterase (BuChE) [4]. Radiolabelled donepezil can thus be used as a tracer to measure brain concentrations of AChE. If the distribution of donepezil in the brain can be measured quantitatively by PET, this will be useful for pharmacological evaluation of AChEIs and for prediction of efficacy of treatment with donepezil. In this study, we performed PET examinations using [5-^{11}C-methoxy]-donepezil ([^{11}C]-donepezil) and determined the *in vivo* binding characteristics of donepezil in AD patients.

Methods

Subjects and patients

Six elderly normal subjects and 10 patients with probable AD were studied to examine the distribution of [^{11}C]-donepezil in the brain. The AD patients were recruited through The Tohoku University Hospital Dementia Patients Registry. The diagnosis of AD was made according to the National Institute of Neurologic Disorders and Stroke/Alzheimer's Disease and Related Disorders Association (NINCDS-ADRDA) criteria. AD patients were further divided into two groups by severity: a mild AD group ($n = 5$; MMSE score ≥ 23 points) and a moderate AD group ($n = 5$; MMSE score < 20 points). The normal control group was comprised of volunteers without impairment of cognitive function who had no cerebrovascular lesions on magnetic resonance (MR) images. After complete description of the study to the patients and subjects, written informed consent was obtained from them. PET study was performed within 3 months after the completion of a medical and neuropsychological examination. Although no significant difference in age was observed between the mild AD group and elderly normal group, the moderate AD group was older than the elderly normal group (Table 1). The

Table 1

Subjects and patients demographics

		Gender	Age	MMSE
Elderly normal	AN1	M	64	30
	AN2	M	61	30
	AN3	F	59	30
	AN4	F	60	30
	AN5	M	74	28
	AN6	F	75	30
	Mean		65.5	29.7
	SD		7.2	0.8
Mild AD	AD1	F	77	24
	AD2	F	72	23
	AD3	M	71	26
	AD4	F	66	25
	AD5	M	69	27
	Mean		71.0	25.0
	SD		4.1	1.6
Moderate AD	AD6	F	77	14
	AD7	F	78	12
	AD8	F	79	19
	AD9	M	84	17
	AD10	F	81	15
	Mean		79.8	15.4
	SD		2.8	2.7

MMSE score of the elderly normal subjects (mean $\pm$ SD 29.7 $\pm$ 0.8) was significantly higher than that of the mild AD (25.0 $\pm$ 1.6) and moderate AD (15.4 $\pm$ 2.7) subjects.

Radiosynthesis of [5-^{11}C-methoxy]-donepezil

Synthesis of [^{11}C]-donepezil was performed (Figure 1) as described previously [5]. Briefly, 5'-O-desmethylprecursor (M2) was dissolved in methylethylketone and then tetrabutylammonium hydroxide was added. [^{11}C]-Methyl iodide was prepared from [^{11}C]-CO$_2$ and converted to [^{11}C]-methyl triflate ([^{11}C]-MeOTf). [^{11}C]-Donepezil was produced on the loop from [^{11}C]-MeOTf and purified by high performance liquid chromatography (HPLC). The radioactivity obtained was 155.4–814 MBq (4.2–22 mCi), and the radiochemical yield was 25–30% based on [^{11}C]-MeOTf after decay-correction. Specific activity was 111–354 GBq µmol^{-1} at the end of synthesis (30–40 min from the end of ^{11}C production). Radiochemical purity was greater than 99%.

PET acquisition protocols

The protocol of the PET study was approved by the Committee on Clinical Investigation at The Tohoku University School of Medicine and the Advisory Committee on Radioactive Substances at Tohoku University. The [^{11}C]-donepezil PET study was performed using a SET-2400 W PET scanner (Shimadzu Inc., Japan) under resting condition with eyes closed. Following a ^{68}Ge/Ga transmission scan of 7 min duration, an emission scan was started soon after intravenous injection of 7.1–9.5 mCi of [^{11}C]-donepezil. Emission
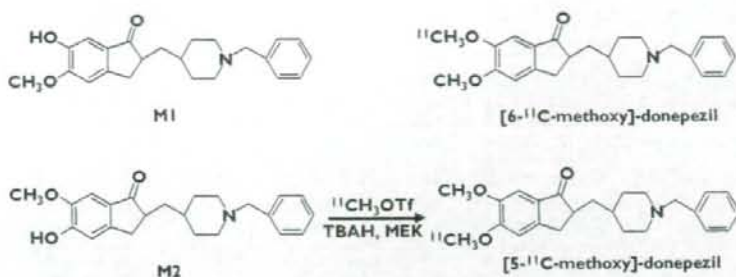
Figure 1
Chemical structures and radiosynthesis of donepezil and its metabolites

data were acquired for 60 min. Standardized uptake value (SUV) images were obtained by normalizing tissue concentration by injected dose and body mass. Arterialized venous blood samples were obtained from a hand vein, heated in a far-infrared mat, and radioactivity was measured in a well-type scintillation counter. Sampled plasma (2 ml) was denatured with 1 M $HClO_4$: MeCN (7 : 3) and centrifuged at $3000 \times g$ for 3 min. The supernatant solution was injected into a column (YMC ODS A-324, YMC Co., Ltd, Kyoto, Japan; 10 mm i.d. $\times$ 30 cm long) with a solvent system of 0.1 M ammonium formate : acetonitrile (60 : 40) at a flow rate of 5.0 ml min^{-1}. The eluates were collected at time intervals of 0.5 min and were counted for radioactivity with a gamma counter.

Image analysis
Region of interest (ROI) analysis was performed to evaluate the regional distribution of [^{11}C]-donepezil. Circular ROIs (1.0 cm in diameter) were placed on individual axial PET images in the cerebellar hemisphere, striatum, thalamus, lateral frontal cortex (Brodmann's areas (BA) 44, 45, 46, and 47), lateral temporal cortex (BA 20, 21, and 22), parietal cortex (BA 39 and 40), occipital cortex (BA 17), anterior cingulate cortex (BA 24 and 32), posterior cingulate cortex (BA 23 and 31), and medial temporal cortex (BA 27, 28, 34, and 35), referring to the individual MR images. To measure donepezil-binding AChE density in the brain, the distribution volume (DV), the ratio of [^{11}C]-donepezil concentration in tissue to that in plasma at equilibrium, was calculated by Logan's graphical analysis [6], since donepezil reversibly binds to AChE. Using this method, the DV in each ROI was determined from the slopes obtained from the values of each ROI and input function from metabolite-corrected plasma radioactivity. The slopes were determined from the last 15 points of the respective regions. Details of the quantitative analysis will be described elsewhere.

Statistical analysis
Differences in age, MMSE score, and DV among the three groups were evaluated by one-way analysis of variance

(ANOVA) followed by Bonferroni's multiple comparison test (GraphPad Prism Software). For each analysis, findings were considered significant at $P < 0.05$.

Results

Tissue time activity curves (TAC) of [^{11}C]-donepezil in the brain indicated initial rapid uptake of radioactivity followed by gradual clearance from the brain in both elderly normal (Figure 2A) and AD subjects (Figure 2B). Relatively high concentrations of radioactivity of [^{11}C]-donepezil were observed in AChE-rich brain regions such as the striatum, thalamus, and cerebellum, whereas radioactivity uptake in the neocortex including frontal, temporal, and parietal cortices was moderate. Plasma radioactivity of [^{11}C]-donepezil peaked at 30–60 s postinjection, followed by a rapid decline (Figure 2C). Proportions of unchanged [^{11}C]-donepezil in plasma were 91.0 ± 7.0%, 88.1 ± 12.5%, and 82.5 ± 5.1% at 5, 15, and 30 min postinjection, respectively. The metabolite-corrected plasma time–activity curve was used to calculate specific DVs from the region-of-interest-derived regional time–activity curve. [^{11}C]-donepezil exhibited linear regression curves on Logan plot analysis in all brain regions examined (Figure 3). Since the slopes of the regression lines represent the DV of the tracer, these findings indicate a higher DV of donepezil in the striatum than in the frontal cortex. Parametric images of [^{11}C]-donepezil DV clearly revealed higher concentrations of tracer distribution in the striatum and cerebellum than in the neocortex. Patients with mild AD exhibited reduction of DV in the hippocampus and neocortex, compared with elderly normal subjects. The magnitude of DV reduction in the mild AD group was about 20% in the hippocampus and 18% in temporal and parietal cortices. In patients with moderate AD, DV reduction was evident throughout the brain (Figure 4, Figure 5, Table 2). The magnitude of DV reduction was about 30% in the hippocampus and 24% in frontal, temporal, and parietal cortices. Two AD patients (AD3 and AD10) underwent another PET scan after treatment with 5 mg donepezil for 6 months. Orally
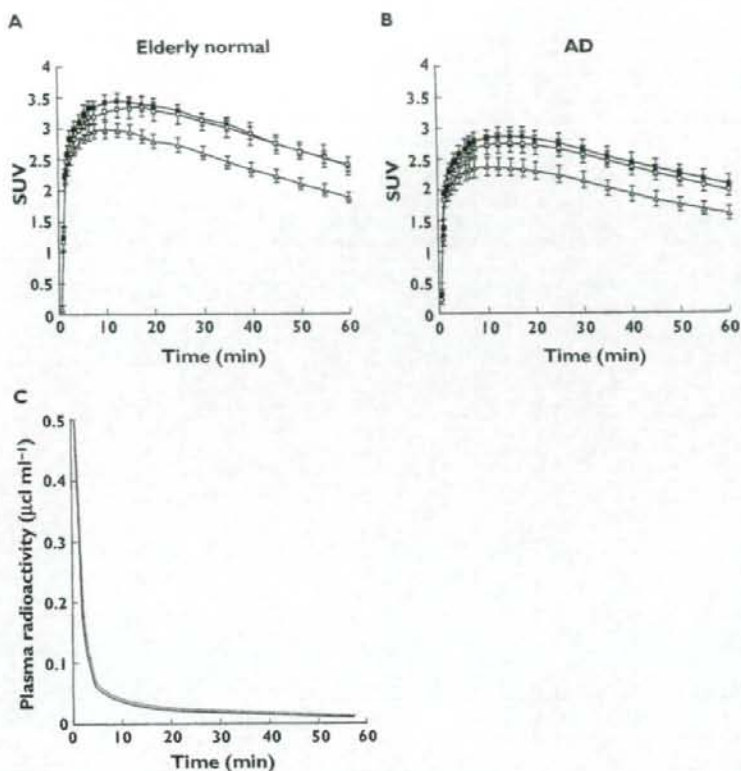
Figure 2

Time activity data for [¹¹C]-donepezil PET in humans. Brain SUV time activity curves for elderly normal subjects (A) and AD patients (B), and plasma time activity curve (C) are shown. The dotted line indicates total time activity curve and the solid line indicates metabolite-corrected time activity curve
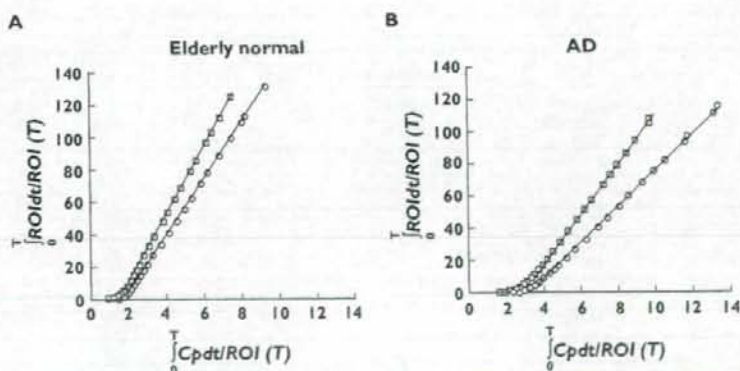

Figure 3

Logan plots for the striatum (□) and frontal cortex (○) for elderly normal subjects (A) and AD patients (B). Cp: plasma concentration of tracer, ROI: region of interest, T: time after injection
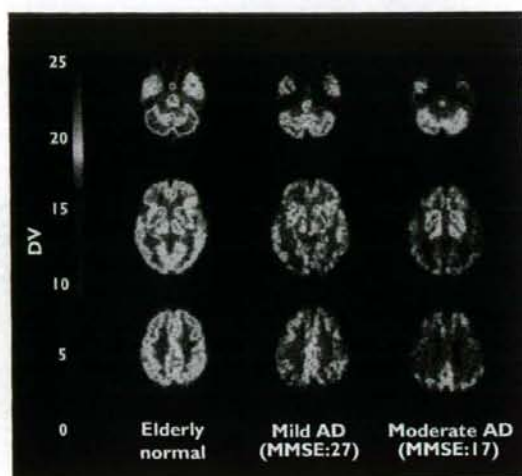
Figure 4

Distribution volume images of [¹¹C]-donepezil in elderly normal subjects (left), patients with mild AD (middle), and patients with moderate AD (right)

administered donepezil induced substantial reduction of DV in all regions of brain examined (Figure 6). Mean DV reduction in patient 1 (AD3) was 61.6% (55.5% in the cerebellum, 65.2% in the striatum, 63.6% in the thalamus, 62.5% in the frontal cortex, 61.6% in the temporal cortex, 59.6% in the parietal cortex, 62.6% in the occipital cortex, 60.3% in the anterior cingulate cortex, 59.5% in the posterior cingulate cortex and 65.5% in the medial temporal cortex). Mean DV reduction in patient 2 (AD10) was 63.3% (59.9% in the cerebellum, 72.0% in the striatum, 60.6% in the thalamus, 61.6% in the frontal cortex, 62.9% in the temporal cortex, 62.4% in the parietal cortex, 54.2% in the occipital cortex, 62.4% in the anterior cingulate cortex, 57.9% in the posterior cingulate cortex and 78.8% in medial temporal cortex). Finally, the correlation of donepezil binding with severity of dementia was examined within the AD patient group. As shown in Figure 7, the DV value in the hippocampus was significantly correlated with MMSE scores of AD patients.

Discussion

Currently, *in vivo* monitoring of brain AChE activity using positron emission tomography (PET) is beneficial in developing strategies for dementia therapy. [¹¹C]-MP4A and [¹¹C]-PMP, which are metabolically trapped acetylcholine analogues, have been successfully applied to the evaluation of AChE activity in the brain [7, 8]. PET studies in AD patients have demonstrated reduction of AChE activity in

the early stage of disease, with the degree of reduction correlating with cognitive dysfunction [9, 10]. Another strategy involves use of AChEls themselves as radiotracers. This method enables direct investigation of the pharmacokinetics of AChEls. [¹¹C]-physostigmine [11], [¹¹C]-methyltacrine [12], and [¹¹C]-CP-126 998 [13] have been designed as radiotracers for clinical PET study. *In vivo* imaging techniques using such radiotracers can measure the concentrations of tracer-binding AChE. If these radiotracers and therapeutic drugs competitively bind to AChE, the occupancy of binding sites on AChE by therapeutic drugs could be measured by subtraction of post-treatment from pretreatment PET scans.

This PET study demonstrated that intravenously administered [¹¹C]-donepezil rapidly enters the brain and is mainly distributed in the striatum, thalamus, and cerebellum, which are known to contain high densities of AChE compared with the cerebral cortex and hippocampus. This finding is consistent with the findings of our previous study in rats [5]. The regional distribution of [¹¹C]-donepezil was also consistent with regional AChE activity determined in a human postmortem study [14], suggesting selective binding of donepezil to AChE.

Post-treatment evaluation following administration of 5 mg donepezil day^{-1} revealed a remarkable reduction (61.6–63.3% compared with pretreatment scan) of [¹¹C]-donepezil binding throughout the brain. This indicates that the AChE occupancy by donepezil, when administered in daily doses of 5 mg, was about 35–40% in these two patients. A previous PET study using [¹¹C]-MP4A revealed a mean 39% reduction in AChE activity after oral administration of 3–5 mg donepezil [15]. Intravenous administration of donepezil in monkeys also resulted in a mean 27% reduction of AChE activity at a dose of 100 µg kg^{-1} [16]. These findings together suggest that inhibition of AChE activity matches occupancy of AChEl binding sites. Moreover, orally administered donepezil (5 mg) induced substantial inhibition (43–62%) of the binding of another radiotracer, [¹¹C]-CP-126 998, to AChE [13]. This finding is roughly consistent with our observations. The amount of binding of orally administered donepezil to AChE is considered a key factor in determining therapeutic response. AChE binding occupancy by orally administered donepezil could be modulated by blood–brain barrier permeability, tissue distribution, metabolism, and also by AChE density in the brain. *In vivo* evaluation of AChE occupancy could thus be a powerful strategy for determining the optimal dose of donepezil. In the future, quantitative evaluation of donepezil binding sites might be used to optimize regimens of treatment with donepezil and to predict the response to treatment. To this purpose, red blood cell AChE inhibition has been explored as a peripheral surrogate marker for the activity of AChEls [17]. In a future study, we plan to examine the relationship between red blood cell AChE inhibition and [¹¹C]-donepezil binding in the brain.
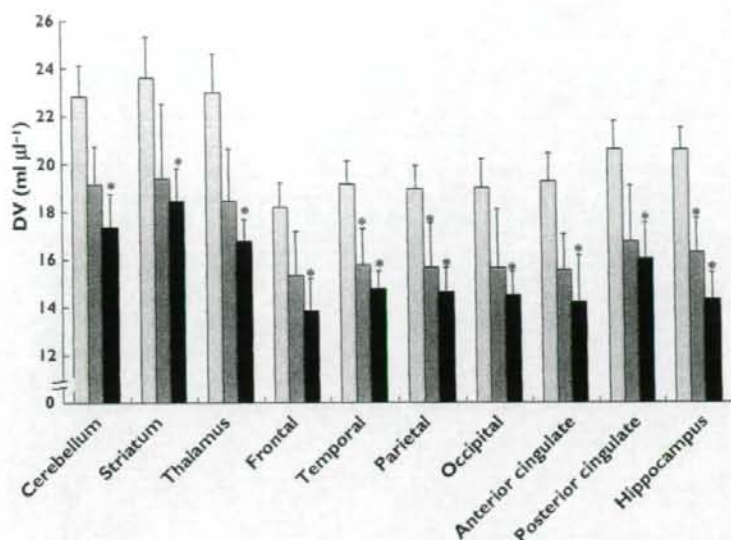
Figure 5

Regional distribution volume data in elderly normal subjects (☐), mild AD (▨), and moderate AD patients (■)

Table 2

Regional distribution volume of [¹¹C]-donepezil in elderly normal subjects and AD patients (mean ± SEM)

	Elderly normal	Mild AD	Moderate AD
Cerebellum	23.4 ± 3.5	19.6 ± 1.4	17.6 ± 1.4*
Striatum	24.0 ± 4.1	20.0 ± 3.1	18.5 ± 1.6*
Thalamus	23.4 ± 4.1	19.0 ± 2.1	17.1 ± 1.0*
Frontal	18.5 ± 2.5	15.8 ± 1.8	14.0 ± 1.5*
Temporal	19.7 ± 2.6	16.2 ± 1.3*	15.1 ± 0.9*
Parietal	19.5 ± 2.7	16.1 ± 1.7*	15.0 ± 1.1*
Occipital	19.4 ± 3.2	16.1 ± 2.3	14.6 ± 1.1*
Anterior cingulate	19.6 ± 2.6	16.2 ± 1.7	14.7 ± 1.9*
Posterior cingulate	21.1 ± 3.0	17.2 ± 2.3	16.3 ± 1.7*
Hippocampus	21.4 ± 2.1	17.3 ± 2.1*	14.8 ± 1.2*

*$P < 0.05$, significantly different from aged normal group.

Figure 6

Distribution volume images before and after oral administration of donepezil in AD patients

Patients with moderate AD exhibited significant reduction of [¹¹C]-donepezil DV in all brain regions examined, in comparison with elderly normal subjects. Furthermore, temporo-parietal and hippocampal DVs were significantly reduced even in patients with mild AD, compared with elderly normal group. These reductions suggest early involvement of the cholinergic system in AD, since the AChE in brain is predominantly located in presynaptic cholinergic neurones [18]. A previous [¹¹C]-MP4A PET study demonstrated 21% reduction of hippocampal AChE activity in patients with early onset AD [19]. We observed a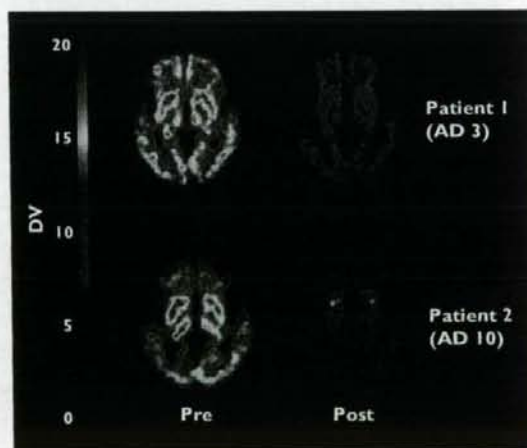n approximately 20% reduction in hippocampal DV in the mild AD group and 30% reduction in the moderate AD group. These findings suggest that the concentration of donepezil-binding AChE is matched by regional AChE activity. In a postmortem study, AD patients exhibited reduction of AChE activity, and this reduction was correlated with the severity of dementia [20, 21]. We observed
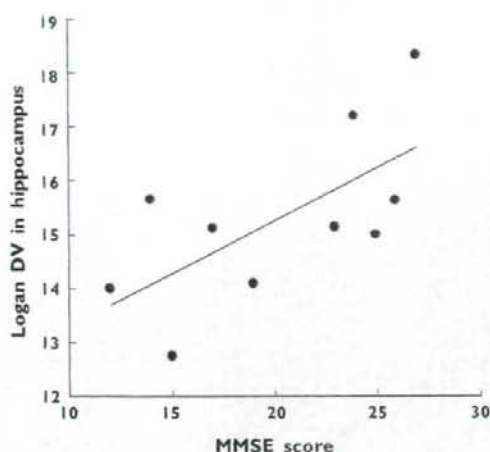
Figure 7

Correlation between MMSE scores and distribution volume in the hippocampus of AD patients. Pearson $r = 0.659$ and $p = 0.038$

that DV in the hippocampus was correlated with the cognitive status in AD patients, a finding in accord with post-mortem data. However, it is important to note that the partial volume effect due to structural atrophy might cause the underestimation of DV in the hippocampus. Analysis after partial volume correction is therefore needed to establish further the relationship between the regional DV of [^{11}C]-donepezil and the severity of dementia in AD.

Compared with previously reported findings of PET imaging with [^{11}C]-MP4A [9] and [^{11}C]-PMP [10], the present [^{11}C]-donepezil-PET study demonstrated a relatively higher cortical retention of radiotracer, suggesting the existence of alternative binding sites for donepezil other than AChE. Donepezil is reported to have high binding affinity for σ_1-receptors, which are widely distributed in the brain including the cerebral cortex, hippocampus, and cerebellum [22–24]. A recent human PET study using a σ_1-receptor-specific radioligand demonstrated prominent reduction of σ_1-receptor density in the cerebral cortex and cerebellum of AD patients [25]. Thus, concomitant binding of donepezil to σ_1-receptors might have contributed to the distinctive distribution of [^{11}C]-donepezil we observed in the brain.

Previously, the tracer kinetics of [^{11}C]-donepezil with labelling of the methoxy group at position 6 ([6-^{11}C-methoxy]-donepezil) were examined in mice and rabbits, to test this agent as a candidate for a PET radioligand [26]. However, the regional brain distribution of this radiotracer did not reflect the distribution of AChE in the brain. In contrast, our previous study yielded successful *in vivo* visualization of AChE by donepezil labelled with ^{11}C at the methoxy group at position 5 ([5-^{11}C-methoxy]-donepezil)

[5]. The differences between these findings might be attributable to the affinity of unlabelled metabolites to AChE. Indeed, the unlabelled metabolite of [6-^{11}C-methoxy]-donepezil (M1 in Figure 1) has high binding affinity for AChE ($IC_{50} = 6.4$ nM), resulting in competition for binding between ^{11}C-labelled tracer and unlabelled metabolite, while the metabolite of [5-^{11}C-methoxy]-donepezil (M2 in Figure 1) exhibits lower affinity of binding to AChE ($IC_{50} = 1.1$ μM) than M1. [5-^{11}C-methoxy]-donepezil is thus suitable for detection of AChE *in vivo*. In addition, the specific radioactivity of [5-^{11}C-methoxy]-donepezil in this study (111–354 GBq μmol^{-1}) was higher than that of [6-^{11}C-methoxy]-donepezil in a previous study [26]. High specific activity of [^{11}C]-donepezil might therefore be another contributing factor of successful visualization of AChE.

In this study, the distribution of donepezil in human brain was successfully visualized using [^{11}C]-donepezil and PET. Graphical analysis by Logan plots can be used to obtain quantitative estimates of specific donepezil binding. AD patients exhibited significant reduction of donepezil distribution, even in the early stages of disease. This imaging technique will be useful as a new surrogate marker for evaluation of treatment with donepezil.

REFERENCES

1 Davies P, Maloney AJ. Selective loss of central cholinergic neurons in Alzheimer's disease. Lancet 1976; 2: 1403.

2 Coyle JT, Price DL, DeLong MR. Alzheimer's disease: a disorder of cortical cholinergic innervation. Science 1983; 219: 1184–90.

3 Giacobini E. Cholinesterase inhibitors: from the Calabar bean to Alzheimer therapy. In: Cholinesterases and Cholinesterase Inhibitors, ed. Giacobini E. London: 2000.

4 Sugimoto H, Ogura H, Arai Y, Iimura Y, Yamanishi Y. Research and development of donepezil hydrochloride, a new type of acetylcholinesterase inhibitor. Jpn J Pharmacol 2002; 89: 7–20.

5 Funaki Y, Kato M, Iwata R, Sakurai E, Sakurai E, Tashiro M, Ido T, Yanai K. Evaluation of the binding characteristics of [5-(11) C-methoxy]-donepezil in the rat brain for *in vivo* visualization of acetylcholinesterase. J Pharmacol Sci 2003; 91: 105–12.

6 Logan J. Graphical analysis of PET data applied to reversible and irreversible tracers. Nucl Med Biol 2000; 27: 661–70.

7 Kilbourn MR, Snyder SE, Sherman PS, Kuhl DE. *In vivo* studies of acetylcholinesterase activity using a labeled substrate, N-[¹¹C]methylpiperdin-4-yl propionate ([¹¹C]PMP). Synapse 1996; 22: 123–31.

8 Irie T, Fukushi K, Namba H, Iyo M, Tamagami H, Nagatsuka S, Ikota N. Brain acetylcholinesterase activity: validation of a PET tracer in a rat model of Alzheimer's disease. J Nucl Med 1996; 37: 649–55.

9 Iyo M, Namba H, Fukushi K, Shinotoh H, Nagatsuka S, Suhara T, Sudo Y, Suzuki K, Irie T. Measurement of acetylcholinesterase by positron emission tomography in the brains of healthy controls and patients with Alzheimer's disease. Lancet 1997; 349: 1805–9.

10 Kuhl DE, Koeppe RA, Minoshima S, Snyder SE, Ficaro EP, Foster NL, Frey KA, Kilbourn MR. *In vivo* mapping of cerebral acetylcholinesterase activity in aging and Alzheimer's disease. Neurology 1999; 52: 691–9.

11 Blomqvist G, Tavitian B, Pappata S, Crouzel C, Jobert A, Doignon I, Di Giamberardino L. Quantitative measurement of cerebral acetylcholinesterase using [¹¹C]physostigmine and positron emission tomography. J Cereb Blood Flow Metab 2001; 21: 114–31.

12 Tavitian B, Pappata S, Bonnot-Lours S, Prenant C, Jobert A, Crouzel C, Di Giamberardino L. Positron emission tomography study of [¹¹C]methyl-tetrahydroaminoacridine (methyl-tacrine) in baboon brain. Eur J Pharmacol 1993; 236: 229–38.

13 Bencherif B, Endres CJ, Musachio JL, Villalobos A, Hilton J, Scheffel U, Dannals RF, Williams S, Frost JJ. PET imaging of brain acetylcholinesterase using [¹¹C]CP-126 998, a brain selective enzyme inhibitor. Synapse 2002; 45: 1–9.

14 Finkelstein Y, Wolff M, Biegon A. Brain acetylcholinesterase after acute parathion poisoning: a comparative quantitative histochemical analysis post mortem. Ann Neurol 1988; 24: 252–7.

15 Shinotoh H, Aotsuka A, Fukushi K, Nagatsuka S, Tanaka N, Ota T, Tanada S, Irie T. Effect of donepezil on brain acetylcholinesterase activity in patients with AD measured by PET. Neurology 2001; 56: 408–10.

16 Shiraishi T, Kikuchi T, Fukushi K, Shinotoh H, Nagatsuka S, Tanaka N, Ota T, Sato K, Hirano S, Tanada S, Iyo M, Irie T. Estimation of plasma IC₅₀ of donepezil hydrochloride for brain acetylcholinesterase inhibition in monkey using N-[¹¹C]methylpiperidin-4-yl acetate ([¹¹C]MP4A) and PET. Neuropsychopharmacology 2005; 30: 2154–61.

17 Sramek JJ, Cutler NR. RBC cholinesterase inhibition: a useful surrogate marker for cholinesterase inhibitor activity in Alzheimer disease therapy? Alzheimer Dis Assoc Disord 2000; 14: 216–27.

18 Mesulam MM, Geula C. Overlap between acetylcholinesterase-rich and choline acetyltransferase-positive (cholinergic) axons in human cerebral cortex. Brain Res 1992; 577: 112–20.

19 Shinotoh H, Namba H, Fukushi K, Nagatsuka S, Tanaka N, Aotsuka A, Ota T, Tanada S, Irie T. Progressive loss of cortical acetylcholinesterase activity in association with cognitive decline in Alzheimer's disease: a positron emission tomography study. Ann Neurol 2000; 48: 194–200.

20 Zubenko GS, Moossy J, Martinez AJ, Rao GR, Kopp U, Hanin I. A brain regional analysis of morphologic and cholinergic abnormalities in Alzheimer's disease. Arch Neurol 1989; 46: 634–8.

21 Prohovnik I, Perl DP, Davis KL, Libow L, Lesser G, Haroutunian V. Dissociation of neuropathology from severity of dementia in late-onset Alzheimer disease. Neurology 2006; 66: 49–55.

22 Kato K, Hayako H, Ishihara Y, Marui S, Iwane M, Miyamoto M. TAK-147, an acetylcholinesterase inhibitor, increases choline acetyltransferase activity in cultured rat septal cholinergic neurons. Neurosci Lett 1999; 260: 5–8.

23 Guitart X, Codony X, Monroy X. Sigma receptors: biology and therapeutic potential. Psychopharmacology 2004; 174: 301–19.

24 Sakata M, Kimura Y, Naganawa M, Oda K, Ishii K, Chihara K, Ishiwata K. Mapping of human cerebral sigma1 receptors using positron emission tomography and [¹¹C]SA4503. Neuroimage 2007; 35: 1–8.

25 Hashimoto K, Ishiwata K. Sigma receptor ligands: possible application as therapeutic drugs and as radiopharmaceuticals. Curr Pharm Des 2006; 12: 3857–76.

26 De Vos F, Santens P, Vermeirsch H, Dewolf I, Dumont F, Slegers G, Dierckx RA, De Reuck J. Pharmacological evaluation of [¹¹C]donepezil as a tracer for visualization of acetylcholinesterase by PET. Nucl Med Biol 2000; 27: 745–7.

Effects of a sedative antihistamine, D-chlorpheniramine, on regional cerebral perfusion and performance during simulated car driving[†]

Manabu Tashiro[1,4]*, Yumiko Sakurada[1,2], Hideki Mochizuki[1], Etsuo Horikawa[3,5], Masahiro Maruyama[3], Nobuyuki Okamura[1], Shoichi Watanuki[4], Hiroyuki Arai[3], Masatoshi Itoh[4] and Kazuhiko Yanai[1,4]

[1]*Department of Pharmacology, Tohoku University Graduate School of Medicine, Sendai, Japan*
[2]*Department of Anesthesiology, Tohoku University Graduate School of Medicine, Sendai, Japan*
[3]*Department of Geriatrics and Gerontology, Tohoku University Graduate School of Medicine, Sendai, Japan*
[4]*Division of Cyclotron Nuclear Medicine, Cyclotron and Radioisotope Centre, Tohoku University, Sendai, Japan*
[5]*Faculty of Medicine, Centre for Comprehensive and Community Medicine, Saga University, Saga, Japan*

Objectives The sedative side effects of antihistamines have been recognized to be potentially dangerous in car driving, but the mechanism underlying these effects has not yet been elucidated to date. The aim of the present study is to examine regional cerebral blood flow (rCBF) responses during a simulated car-driving task following oral administration of D-chlorpheniramine using positron emission tomography (PET) and $[^{15}O]H_2O$, based on a single-blind cross-over study-design.
Methods Right-handed, healthy male volunteers ($n = 14$) drove a car in a simulated environment following oral administration of D-chlorpheniramine repetab 6 mg or placebo. Their rCBF was measured using PET with $[^{15}O]H_2O$ in the following three conditions: (1) resting, (2) active driving, and (3) passive driving. All 'in-car' views during the simulated driving were videotaped and used for rating driving performance.
Results Performance evaluation revealed that the number of lane deviations significantly increased in the D-chlorpheniramine condition compared with the placebo condition ($p < 0.01$). Subjective sleepiness was not significantly different between the two drug conditions. The regions of diminished brain responses following D-chlorpheniramine treatment were detected in the parietal, temporal and visual cortices, and in the cerebellum. The regions of augmented rCBF responses were found in the orbitofrontal cortex and cerebellar vermis.
Conclusion These results suggest that D-chlorpheniramine tends to suppress visuo-spatial cognition and visuo-motor coordinating functions rather than attention and motor functions during car driving. Copyright © 2008 John Wiley & Sons, Ltd.

KEY WORDS — antihistamine; impaired performance; cerebral blood flow; PET; car driving

INTRODUCTION

Car driving is one of our everyday tasks and is also a series of complex perceptual and psychomotor tasks

* Correspondence to: M. Tashiro, Division of Cyclotron Nuclear Medicine, Cyclotron and Radioisotope Centre, Tohoku University, Aoba 6-3, Aramaki, Aoba-ku, Sendai, Miyagi 980-8578, Japan.
Tel: +81-22-795-7797. Fax: +81-22-795-7797.
E-mail: mtashiro@mail.tains.tohoku.ac.jp
†Yumiko Sakurada contributed equally to this work.

that require the integration of various basic functions such as attention, visuo-spatial cognition, motor programming and control, and visuo-motor coordination (Theunissen *et al.*, 2004; Verster and Volkerts, 2004). Cognitive and psychomotor impairments following the administration of sedating drugs can lead to impairment of driving performance and increase a driver's risk of injury (Movig *et al.*, 2004; Seppala *et al.*, 1979). So far, a large number of studies have been conducted to determine the effects on driving behavior following administration of